Rend. Mat. Appl. (7).
Volume 39 (2018), 347 – 362

RENDICONTI DI MATEMATICA
E DELLE SUE APPLICAZIONI

Non-linear Gross-Pitaevskii dynamics of a 2D binary condensate: a numerical analysis

Alessandro Michelangeli and Giuseppe Pitton

Dedicated to Gianfausto Dell'Antonio on the occasion of his 85th birthday

Abstract. *We present a numerical study of the two-dimensional Gross-Pitaevskii systems in a wide range of relevant regimes of population ratios and intra-species and inter-species interactions. Our numerical method is based on a Fourier collocation scheme in space combined with a fourth order integrating factor scheme in time.*

1 Background and outline

We are concerned in this work with the following system of two coupled cubic non-linear Schrödinger equations

$$\begin{aligned} \mathrm{i}\,\partial_t u &= -\Delta u + Uu + \gamma_1|u|^2u + c_2\gamma_{12}|v|^2u \\ \mathrm{i}\,\partial_t v &= -\Delta v + Uv + \gamma_2|v|^2v + c_1\gamma_{12}|u|^2v\,, \end{aligned} \tag{1.1}$$

in the complex-valued unknowns $u \equiv u(\mathbf{x},t)$ and $v \equiv v(\mathbf{x},t)$ with $t \in \mathbf{x}$ and $\mathbf{x} \in \mathbb{R}^2$, and for given parameters $\gamma_1, \gamma_2, \gamma_{12} \in \mathbb{R}$ ('interaction couplings'), $c_1, c_2 \in [0,1]$ with $c_1 + c_2 = 1$ ('population ratios'), and given $U : \mathbb{R}^2 \to \mathbb{R}$ ('trapping potential'): such a system is customarily referred to as the *Gross-Pitaevskii system*, and we present here a systematic numerical analysis of the solutions to (1.1) for typical initial data (u_0, v_0) at $t = 0$ and typical choices of the parameters, in view of the physical applications.

In fact, (1.1) describes to a good approximation and in suitable units the *effective* dynamics of a binary mixture of Bose-Einstein condensates in a mean-field-type limit of large number of particles and high dilution, in the sense, that can be made precise, that the actual solution of the many-body Schrödinger dynamics behaves approximately as the uncorrelated product of identical one-body 'orbitals' u (the quantum mechanical wave-function for a particle of the fist type) for one species of the mixture and one-body orbitals v for the other species.

2010 Physics and Astronomy Classification Scheme: 02.30.Jr, 02.60.Cb, 02.70.Hm, 02.70.Jn, 67.85.De, 67.85.Fg.

Keywords: Bose-Einstein condensation, multi-component mixtures, non-linear Gross-Pitaevskii system, Fourier pseudo-spectral method; integrating factor method.

Let us recall that binary mixtures of condensates [24, 18, 11] are gaseous mixtures of two distinguishable species of bosons, which coexist in the same spatial region and display Bose-Einstein condensation in each component, and where interactions are present both between particles of the same species and of different species, however with no inter-species transition. Today such systems can be prepared and manipulated in a wide range of current experiments with cold atoms, typically involving heteronuclear mixtures such as ^{41}K–^{87}Rb [22], ^{41}K–^{85}Rb [23], ^{39}K–^{85}Rb [19], ^{85}K–^{87}Rb [26].

The drastic simplification of the effective description (1.1) is clear from the fact that it consists of two PDE's for *one* pair only of orbitals (u, v) instead of a PDE (the many-body linear Schrödinger equation) in a time-dependent unknown function of $N_1 + N_2$ two-dimensional space variables, where N_1 and N_2 are the number of particles in each component of the condensate and can be of the order of 10^4 through 10^{11}. The effective description retains track of the population ratios through the coefficients $c_j = N_j/(N_1 + N_2)$, $j \in \{1, 2\}$, and of the intra-species and inter-species scattering lengths, proportional respectively to γ_1, γ_2 and to γ_{12}, besides the presence of the typical cubic non-linearities that are naturally interpreted as self-interaction terms.

We remark that for the *two-dimensional* problem (1.1) we are considering the structure of the *three-dimensional* Gross-Pitaevskii system, thus in practice we are thinking of a Bose mixture confined in a thin planar slice, but before the genuine 2D limit is taken.

An intense activity has been flourishing recently on the mathematical formalisation of Bose mixtures and binary condensates, the rigorous derivation of the effective dynamics, and the study of the ground state properties: we refer to the works [1, 21, 20, 25] for a thorough discussion.

On the other hand, the local and global well-posedness of the Cauchy problem for (1.1) and related features of the solutions, has been deeply investigated in the mathematical literature of the last decade, in particular in the works [16, 10, 17, 8, 15, 13].

From the numerical side, the analysis is less developed and we shall provide references in a moment. Remarkably, systematic numerics of various types of collisions between the condensate components, including symmetric and asymmetric collisions followed by ballistic expansion, as well as repeated collisions in a trap, are missing in the literature. The aim of this work is precisely to close this gap.

2 Numerical analysis: methods

The single-component Gross-Pitaevskii equation has been extensively studied numerically over the last 20 years, mostly using Fourier [3, 4], Spherical Harmonics [28] and Laguerre-Hermite [5] spectral methods, and operator splitting for the integration in time. For a review of the most popular numerical approaches to the single-component Gross-Pitaevskii equation we refer to [2].

The two-component case is less studied, although some relevant works have appeared in the last 15 years, mostly based on hybrid finite difference-Fourier spectral methods coupled with Crank-Nicolson or second order (Strang) splitting in time [30]. Spherical Harmonic [28] and Laguerre [29] spectral methods have also been exploited, coupled with a second order operator splitting in time.

The case of a rotating binary condensate is well studied in the literature, and we do not discuss it here, referring instead to [2, 31].

The standard resolution adopted in the previous works is insufficient for our goals and, in order to resolve relevant short-scale details of the dynamics, we wrote an MPI-parallel code.

For the numerical solution of the initial value problem associated with the system (1.1) we chose a Fourier collocation method [7] in space (sometimes called Fourier pseudo-spectral method) combined with a fourth-order integrating factor method in time, first introduced in [6].

2.1 Accuracy check

The accuracy of the numerical solution is controlled in two ways. The accuracy in space is checked by inspecting the magnitude of the Fourier coefficients, and making sure that all the Fourier coefficients with magnitude larger than a given threshold (that we take equal to 10^{-6}) are represented. The accuracy in time is checked by making sure that the L^2-norm of both components lies within a band of $\pm 10^{-5}$ times the L^2-norm of the initial datum.

2.2 Initial data

In all our simulations we choose for each component an initial profile of Gaussian type, namely the (L^2-normalised) wave-function

$$G_{\mathbf{q},\mathbf{p},\theta}(\mathbf{x}) \;:=\; \frac{1}{\theta\sqrt{\pi}}\, \mathrm{e}^{\mathrm{i}\mathbf{p}\cdot\mathbf{x}}\, \exp\left(-\frac{|\mathbf{x}-\mathbf{q}|^2}{2\theta^2}\right) \tag{2.1}$$

centred at position $\mathbf{q}$ with momentum $\mathbf{p}$ and spread θ.

The normalisation $\|G_{\mathbf{q},\mathbf{p},\theta}\|_2 = 1$ is consistent with the choice of the coefficients, and in particular the presence of the population factors c_1 and c_2, in the system (1.1), namely the two orbitals u and v are normalised to 1. The connection, by a re-scaling, with the 'physical' normalisation $\|u\|_2^2 = \|v\|_2^2 = 1$, is discussed exhaustively in [21, Sect. 4].

This is a physically relevant choice, since $G_{\mathbf{q},\mathbf{p},\theta}$ is preparable as the ground state of a suitable harmonic trap when the interaction is sufficiently weak, and besides that it can be thought of as the outcome of modern wave-function engineering [11, Section 16.2.4]. Furthermore, this choice is versatile for an amount of numerical simulations: choosing for u_0 and v_0 different $\mathbf{q}$'s and $\mathbf{p}$'s allows one

Table 1: Initial data parameters for the simulations of one-shot scattering (Section 3.1), component-over-component relaxation (Section 3.2), and harmonically trapped re-collisions (Section 3.3)

	scattering and re-collisions						relaxations					
	θ	p_x	p_y	q_x	q_y		θ	p_x	p_y	q_x	q_y
u_0	0.05	-100	0	5θ	0	u_0	0.05	0	0	$\theta/2$	0
v_0	0.05	100	0	-5θ	0	v_0	0.05	0	0	$-\theta/2$	0

Table 2: Parameters for the head-on scattering simulations

n	γ_1	γ_2	γ_{12}	c_1	c_2	$\triangle + 1$	N
1	1	1	10^3	0.50	0.50	$4.00 \cdot 10^{-6}$	2^{12}
2	1	1	10^3	0.10	0.90	$1.11 \cdot 10^{-5}$	2^{12}
3	1	1	10^3	0.01	0.99	$1.01 \cdot 10^{-4}$	2^{12}
4	10^3	10^3	10^3	0.50	0.50	4	2^{13}
5	1	1	-200	0.50	0.50	$1 \cdot 10^{-4}$	2^{11}
6	-1	-1	200	0.50	0.50	$1 \cdot 10^{-4}$	2^{11}

to simulate various kinds of head-on collisions with zero or non-zero impact parameter, taking instead $\mathbf{p} = \mathbf{0}$ and the same $\mathbf{q}$ for both u_0 and v_0 allows one to simulate the relaxation of one component on top of the other, and so on.

Table 1 lists the pool of the initial parameters $(\mathbf{q}, \mathbf{p}, \theta)$ that we considered for the numerical experiments of head-on scattering (Section 3.1) and of multiple re-collisions (Section 3.3) between the two components of the condensate. Table 1 lists the initial parameters for the numerical experiments of component-over-component relaxation (Section 3.2).

We tuned such values so as to guarantee, thanks to a strong enough Gaussian decay of the initial profiles u_0 and v_0, that the initial data are well localised within the spatial domain and in Fourier momentum, and to guarantee also that for all the duration of our numerical experiments the accuracy criteria of Section 2.1 are matched.

3 Numerical analysis: results

In this Section we report and discuss the results of three main groups of numerical experiments.

We test a wide range of possible regimes, which include balanced ($c_1 = c_2$), mildly unbalanced ($c_1 \lesssim c_2$), and strongly unbalanced ($c_1 \ll c_2$) population ratios, as well as intra-species and inter-species interactions ($\alpha \in \{1, 2, 12\}$), of both repulsive ($\gamma_\alpha > 0$) and attractive ($\gamma_\alpha < 0$) type. We also explore various magnitudes

of the *miscibility parameter*

$$\triangle := \frac{\gamma_1\gamma_2}{c_1c_2\gamma_{12}^2} - 1 \tag{3.1}$$

that discriminates between spatial phase mixing ($\triangle > 0$) or phase separation ($\triangle < 0$) in the ground state associated with our non-linear system (1.1) [27, Section 21.1], and which determines also the blow-up threshold of the associated initial value problem.

3.1 One-shot, head-on scattering

The first class of experiments we investigate are one-shot collisions of the two components of a binary condensate initially prepared with a sharp spatial separation and a relative velocity against each other, and left free to scatter away after they have come on top of each other.

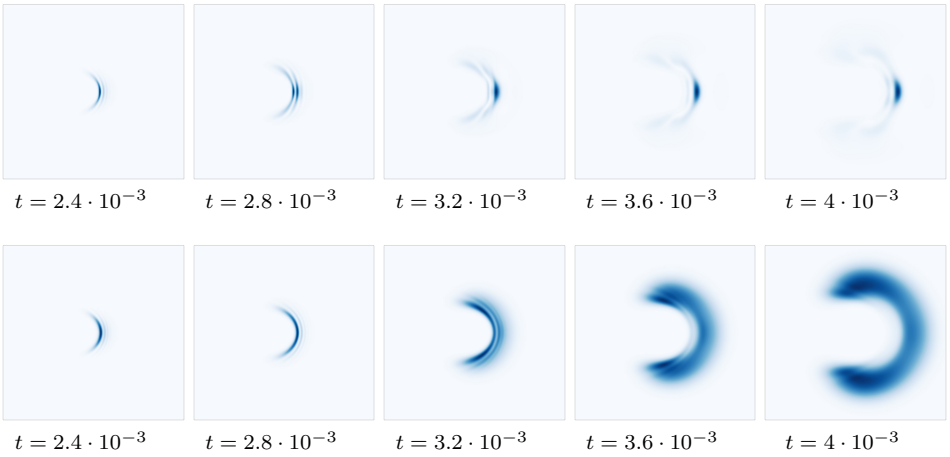

Figure 1: Density profile $|u(\mathbf{x}, t)|^2$ during the head-on scattering between components: experiments $n = 2$ (top) and $n = 3$ (bottom) of Table 2, with the same interaction parameters but increasing unbalance $c_1 = 0.10, 0.01$. For visualization purposes, along each row the magnitude scale changes (see Fig. 3).

Conventionally (see Table 1) we let the scattering process to take place along the x-axis of our spatial grid and we take the u-component to be initially shot from right to left, the v-component then shot from left to right. Here $U \equiv 0$: each component of the condensate is free to expand ballistically.

In a sequence of numerical experiments (cases $n = 1, 2, 3$ of Table 2) we explore the effects of an increasing unbalance in the population ratios on the head-on scattering process with *repulsive* intra-species *and* inter-species interactions, where the two components are initially shot against each other with momenta of equal

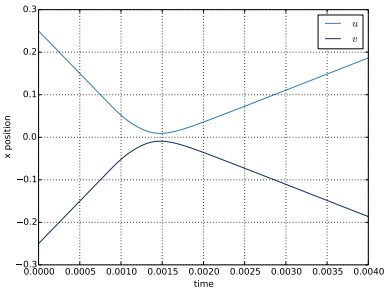

$(n = 1) \quad c_1 = c_2 = 0.50$
$\gamma_1 = \gamma_2 = 1,\ \gamma_{12} = 10^3$

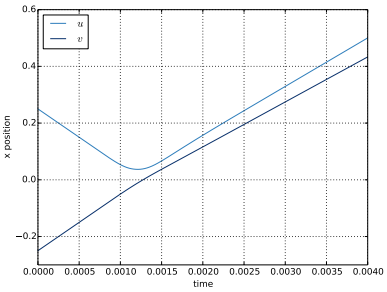

$(n = 2) \quad c_1 = 0.10,\ c_2 = 0.90$
$\gamma_1 = \gamma_2 = 1,\ \gamma_{12} = 10^3$

Figure 2: Time behaviour of the average positions $\mathbf{X}_u(t)$ and $\mathbf{X}_v(t)$ (along the x-axis of the spatial grid) of each component of a binary condensate during the head-on scattering process between components, relative to the numerical experiments $n = 1, 2$ from Table 2. An effect emerges of the population unbalance.

magnitude and opposite sign. This can be seen to ensure the system (1.1) to be well posed in H^1 globally in time [13]. In Figure 1 we show that the lower the relative population of the u-component, and hence the lighter the u-condensate, the more its localisation in space is destroyed during the recoil: the density of the u-condensate gets spread in a remarkable pattern around the density of the much more populated (heavier) v-condensate, which instead remains well localised in space. Figure 2 supplements this picture in terms of the average positions of each components, that is, the vectors

$$\mathbf{X}_u(t) \;:=\; \int_{\mathbb{R}^2} \mathbf{x}\,|u(\mathbf{x},t)|^2\,\mathrm{d}\mathbf{x}\,, \qquad \mathbf{X}_v(t) \;:=\; \int_{\mathbb{R}^2} \mathbf{x}\,|v(\mathbf{x},t)|^2\,\mathrm{d}\mathbf{x}\,. \tag{3.2}$$

The plot of the horizontal components (x-components) of $\mathbf{X}_u$ and $\mathbf{X}_v$ shows that for balanced or almost balanced populations both components recoil, whereas when the unbalance increases the heavier component preserves its localisation and proceeds along a direction only slightly changed after the collision.

The same head-on collisions with various degree of unbalance in the population ratios (cases $n = 1, 2, 3$ of Table 2) are further studied by monitoring the behaviour in time of the norms $\|u(\cdot,t)\|_\infty$ and $\|v(\cdot,t)\|_\infty$. In fact, the profiles of $|u(\mathbf{x},t)|$ and $|v(\mathbf{x},t)|$ develop peaks when a concentration of mass occurs, significantly when the two components come spatially on top of each other: the L^∞-norm captures the appearance of such peaks. In Figure 3 we show that sufficiently far in time before or after the actual collision phase the L^∞-norm of each component decreases with a typical dispersive behaviour, and this happens for any population ratio. During the collision phase, instead, the L^∞-norm undergoes a rapid increase, followed by a somewhat less rapid decrease. Moreover, the lighter a component, the more pronounced is the jump of its L^∞-norm.

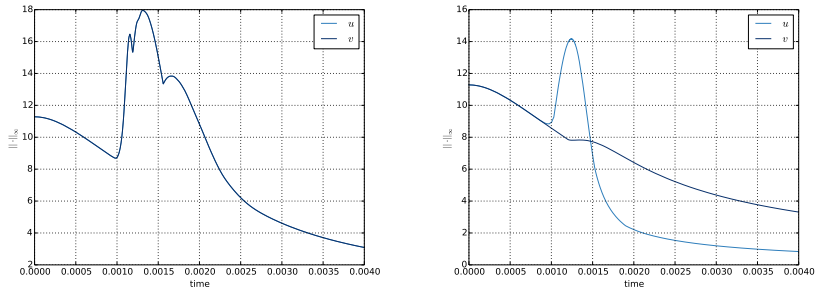

$(n = 1)$ $c_1 = c_2 = 0.50$
$\gamma_1 = \gamma_2 = 1$, $\gamma_{12} = 10^3$

$(n = 3)$ $c_1 = 0.01$, $c_2 = 0.99$
$\gamma_1 = \gamma_2 = 1$, $\gamma_{12} = 10^3$

Figure 3: Time behaviour of the norms $\|u(\cdot,t)\|_\infty$ and $\|v(\cdot,t)\|_\infty$ during the head-on scattering process between the two components of a binary condensate, relative to the numerical experiments $n = 1$ (left) and $n = 3$ (right) from Table 2.

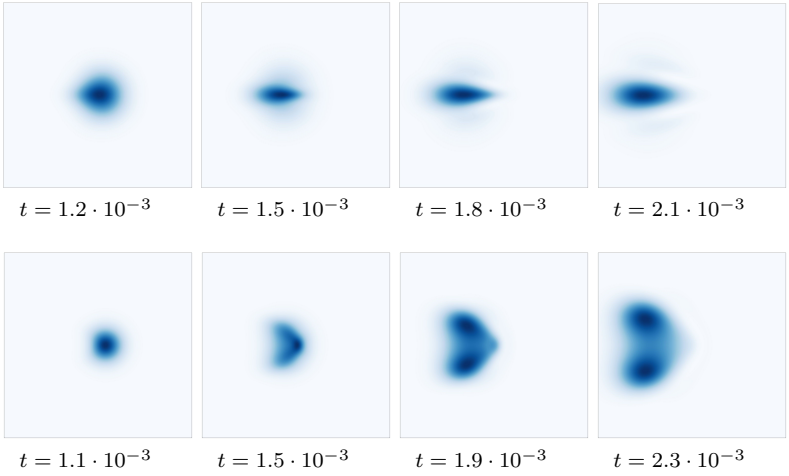

$t = 1.2 \cdot 10^{-3}$ $t = 1.5 \cdot 10^{-3}$ $t = 1.8 \cdot 10^{-3}$ $t = 2.1 \cdot 10^{-3}$

$t = 1.1 \cdot 10^{-3}$ $t = 1.5 \cdot 10^{-3}$ $t = 1.9 \cdot 10^{-3}$ $t = 2.3 \cdot 10^{-3}$

Figure 4: Density profile $|u(\mathbf{x},t)|^2$ during the head-on scattering between two equally populated components. Top: 'Squeezing-and-shooting' effect for the experiment $n = 5$ of Table 2. Bottom: 'Splash-the-blob' effect of the experiment and $n = 6$. The scale changes in each frame.

We then turn to explore the effects of different magnitudes of the intra- and inter-species interactions when the collision takes place between components of equal populations. Two paradigmatic patterns emerge. When an *attraction* between the two components is present, of significantly stronger magnitude than the intra-species coupling (be the latter positive or negative), a characteristic 'squeezing-and-shooting' effect occurs in which the two profiles undergo a very

quick and pronounced contraction in the region of spatial overlap, followed by the ejection of two very much focused and elongated wave packets in opposite directions (numerical experiment $n = 5$ in the first two rows of Figure 4). Instead, when between the two components a *repulsion* is present of much stronger magnitude than the inter-species coupling, this results in a 'splash-the-blob' effect caused by the violent expansion of the two profiles under the the strong repulsion occurring at the moment of their spatial overlap, thus followed by a wide spread of each cloud and possibly by the production of two distinct upper and lower sub-clouds with respect of the incident direction (numerical experiment $n = 6$ in Figure 4).

Table 3: Parameters for the relaxation simulations

n	γ_1	γ_2	γ_{12}	c_1	c_2	$\triangle + 1$	N_0
7	1	1	10^3	0.50	0.50	$4 \cdot 10^{-6}$	2^{10}
8	1	1	10^3	0.01	0.99	10^{-4}	2^{11}
9	-10^3	-10^3	-10^3	0.50	0.50	4	2^{12}
10	-10^3	-10^3	-10^3	0.01	0.99	101	2^{12}

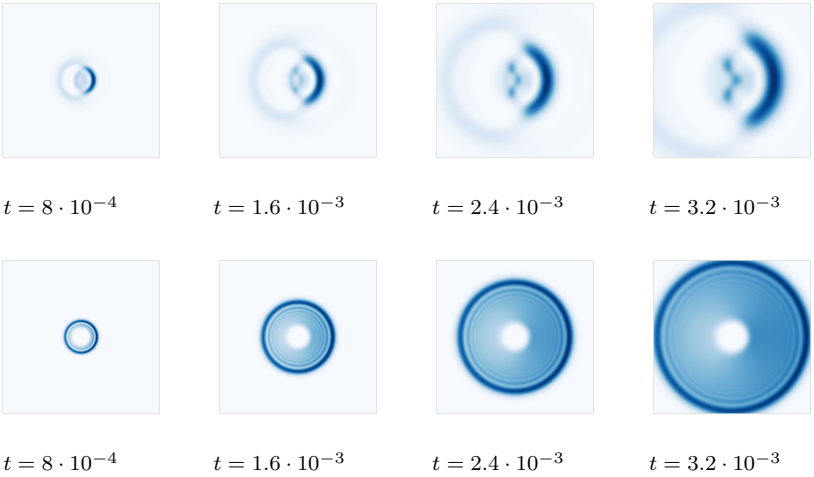

Figure 5: Light component's density profile $|u(\mathbf{x}, t)|^2$ at various times during the relaxation over the heavy component in a binary condensates: numerical experiments $n = 7, 8$ of Table 3, both with interaction couplings $\gamma_1 = \gamma_2 = 1$, $\gamma_{12} = 10^3$), and increasing unbalance $c_1 = 0.50$ (top) and $c_1 = 0.01$ (bottom). For visualization purposes, the scale changes in each frame.

3.2 Condensate-over-condensate relaxation

The second class of experiments we investigate are the relaxations of one component over the other in a binary condensate with both populations initially localised

in the same region. Also in this case we take $U \equiv 0$, that is, the relaxation is not trapped.

In order to magnify the relevant features of the dynamics, we introduce a small displacement between the centres of the Gaussian profiles of the initial data, with the u-component (resp., the v-component) slightly shifted to the right (resp., to the left) along the x-axis. Each profile has zero momentum at the beginning. The precise initial conditions and the simulation parameters are summarised in Tables 1 and 3.

Several competing effects enter the relaxation process: the dispersive nature of the kinetic operator in the system (1.1) favours a gradual spread in space of the solutions, repulsive interactions (de-focusing couplings) enhance further this effect whereas attractive interactions (focusing couplings) tend to contrast it, and the relative balance between intra-species and inter-species interactions, encoded in the parameter $\triangle$ defined in (3.1) further pushes towards reinforcing or suppressing the expansion of the two clouds.

In a first round of simulations we explore the effects of an increasing unbalance in the population ratios on the relaxation process, in the presence of repulsive interactions among particles of any type, and where the inter-species repulsion has a much stronger magnitude than the intra-species one.

In Figure 5 we show that when the two components are (almost) equally populated the corresponding profiles separate and disperse gradually in time, with an asymmetric spatial distribution that reflects the asymmetry of the configuration at time $t = 0$: thus, the u-component goes shifted away to the right, and the v-component to the left. The more the population ratios become unbalanced, the slower and more symmetrically the profile of the heavy component spreads, pushing away the light component around it. In this regime, the strong unbalance between heavy and light component overcomes relatively soon the spatial asymmetry of the initial configuration: the two clouds expand radially, the heavier one well localised around the initial position, the lighter one pushed away in an annulus around the heavier with several circular waves following the main wave, which become more packed as γ_{12} increases.

All this provides a novel and more structured evidence of the dynamical formation of phase separation in the non-miscibility regime $\triangle < 0$ for a binary condensate, an experimental feature [12, 11] that has been partially reproduced by recent numerical studies [9, 14].

We further analyze the relaxation process through the behaviour of the average positions $\mathbf{X}_u(t)$ and $\mathbf{X}_v(t)$, both under a change in the interactions and in the population ratios (Figure 6). In the repulsive regime, the lighter one component, the faster it gets pushed away from the heavy one, which remains instead almost steady, whereas with comparable population ratios the two profiles get far apart almost symmetrically. Remarkably, when instead intra-species and inter-species interactions are turned to attractive and with comparable magnitude, this results in an appreciable competing effect against the dispersion induced by the linear part of the dynamics and in a much slower speed separation. For example, comparing

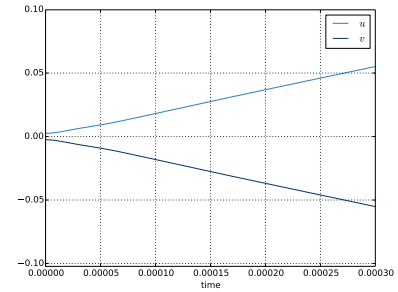

$(n = 7)$ $c_1 = 0.50$, $c_2 = 0.50$
$\gamma_1 = \gamma_2 = 1\,,\quad \gamma_{12} = 10^3$

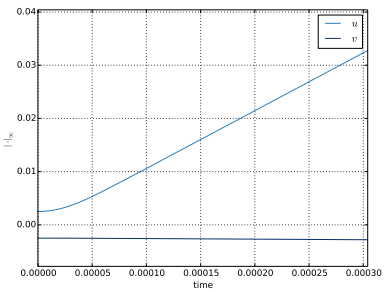

$(n = 8)$ $c_1 = 0.01$, $c_2 = 0.99$
$\gamma_1 = \gamma_2 = 1\,,\quad \gamma_{12} = 10^4$

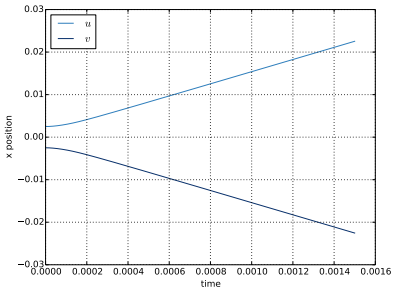

$(n = 9)$ $c_1 = 0.50$, $c_2 = 0.50$
$\gamma_1 = \gamma_2 = \gamma_{12} = -10^3$

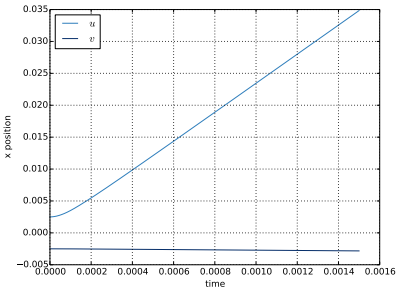

$(n = 10)$ $c_1 = 0.01$, $c_2 = 0.99$
$\gamma_1 = \gamma_2 = \gamma_{12} = -10^3$

Figure 6: Time behaviour of the average positions $\mathbf{X}_u(t)$ and $\mathbf{X}_v(t)$ (along the x-axis of the spatial grid) of each component of a binary condensate during the component-over-component relaxation, experiments $n = 7, 8, 9, 10$ of Table 3.

the cases $n = 7$ and $n = 9$ in Figure 6, both with equal populations, it takes a 10 times longer period in the second case (competing attraction, slow separation) for $|\mathbf{X}_u(t) - \mathbf{X}_v(t)|$ to attain the same value as in the first case (repulsion and hence fast separation).

3.3 Multiple re-collisions for a harmonically trapped binary condensate

As a third class of simulations, we consider the component-component multiple re-collisions occurring in a harmonically trapped binary condensate.

The initial data (Table 1) are the same as those used for the single-collision simulations, that is, two components shot against each other. The system (1.1) is now solved with the harmonic potential

$$U(\mathbf{x}) \;=\; \omega^2|\mathbf{x}|^2\,, \qquad \omega = 10^2\,, \tag{3.3}$$

Table 4: Parameters for the harmonically trapped re-collision simulations.

n	γ_1	γ_2	γ_{12}	c_1	c_2	$\triangle + 1$	N_0
11	1	1	10^3	0.50	0.50	$4 \cdot 10^{-6}$	2^{13}
12	1	1	10^3	0.10	0.90	$1.1 \cdot 10^{-5}$	2^{13}
13	1	1	10^3	0.01	0.99	10^{-6}	2^{13}
14	1	1	$5 \cdot 10^3$	0.50	0.50	$1.6 \cdot 10^{-7}$	2^{13}
15	1	1	-200	0.50	0.50	$1 \cdot 10^{-4}$	2^{12}
16	-1	-1	50	0.50	0.50	$1.6 \cdot 10^{-3}$	2^{11}

with ω chosen by trial and error so that in all the considered experiments the solution profiles remain well localised within the computational grid and the simulations can be resolved numerically. To this aim, we also enlarge the computational domain to $[-2\pi, 2\pi]^2$. The simulation parameters for this series are listed in Table 4 and are chosen among those relevant cases from the single-collision scenario for which our numerics provides the cleanest evidence.

Owing to the harmonic confinement, the two components undergo a pulsing behaviour with re-collisions followed by escapes towards opposite directions. In order to compute several of such events, a considerably longer time integration is required, to achieve which with acceptable accuracy we *reduce the time step* to $h = 2 \cdot 10^{-7}$. With this choice, the relative mass loss exceeds the fidelity threshold of 10^{-5} in approximately $4 \cdot 10^5$ time steps.

Analogously to the single collision case (Section 3.1) in the presence of repulsive interactions, we find that the solutions exhibit a repeated recoil pattern when the two components are equally populated, whereas when a considerably heavier component hits for the first time the much lighter one, the former drags the latter in an almost periodic motion within the trap. The rapid mass concentration occurring at each collision results in a jump of the L^∞-norms of the solutions. These phenomena are visualised in Figure 9.

Pushing further the unbalance in the population ratios, what we had found in the single collision case (last row of Figure 1) was the complete destruction of the localisation of the light component and its almost radial spread, with a larger part of its mass scattered in the direction of the incident heavy component. The confining potential has now the effect to focus the outgoing annular wave of the light component profile back to the centre of the trap, where the cycle is then repeated. After multiple re-collisions the annular wave of the light component deteriorates in several fringes. This phenomenon is visualised in Figure 10.

Last, we analyse the effects of competing interactions on the multiple re-collisions of two equally populated components (Figures 7 and 8). The two most relevant cases are the 'squeezing-and-shooting' scattering realised when the inter-species attraction has a much stronger magnitude than the intra-species repulsion (experiment $n = 15$ of Table 4), and the 'splash' effect realised when the inter-

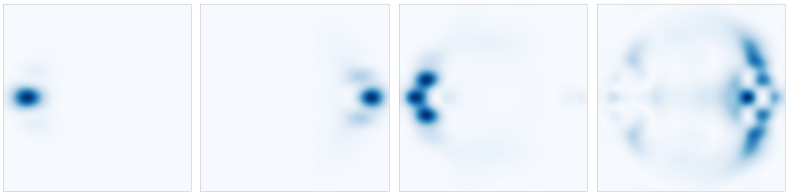

Figure 7: Density profile $|u(\mathbf{x}, t)|^2$ at various times during harmonically trapped recollisions between equally populated components. Top: experiment $n = 15$ of Table 4 with the first four collisions, at the instants of velocity inversion. Bottom: experiment $n = 16$ with the first, third, fifth, and sixth collision. The scale changes along each row (for the absolute scale see Figure 8).

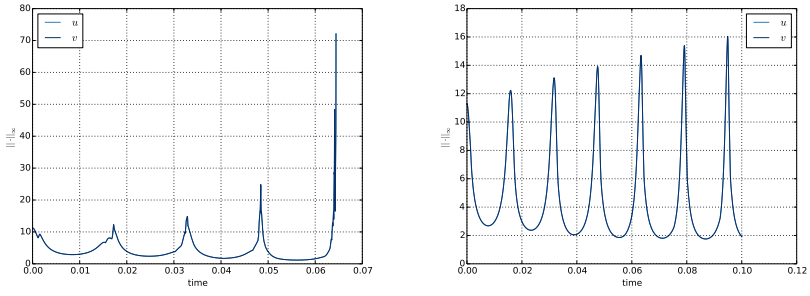

$(n = 15)$ $\gamma_1 = \gamma_2 = 1, \gamma_{12} = -200$ $(n = 16)$ $\gamma_1 = \gamma_2 = -1, \gamma_{12} = 50$

Figure 8: Time behaviour of the norm $\|u(\cdot, t)\|_\infty$ during harmonically trapped recollisions relative to experiments $n = 15$ (left) and $n = 16$ (right) of Table 4. Since the two populations are the same, by symmetry $\|v(\cdot, t)\|_\infty = \|u(\cdot, t)\|_\infty$.

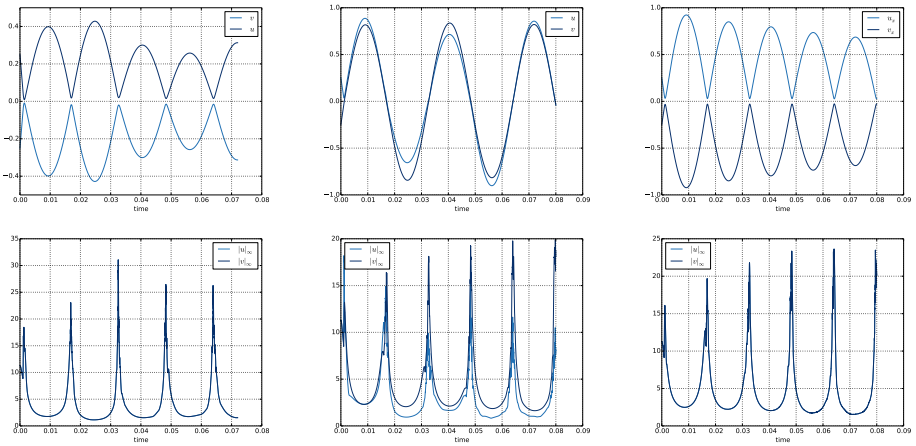

$c_1 = 0.5,\ c_2 = 0.5$
$\gamma_{12} = 10^3,\ \gamma_1 = \gamma_2 = 1$

$c_1 = 0.1,\ c_2 = 0.9$
$\gamma_{12} = 10^3,\ \gamma_1 = \gamma_2 = 1$

$c_1 = 0.5,\ c_2 = 0.5$
$\gamma_{12} = 5 \cdot 10^3,\ \gamma_1 = \gamma_2 = 1$

Figure 9: Time behaviour of the norms $\|u(\cdot,t)\|_\infty$ and $\|v(\cdot,t)\|_\infty$ (top row) and of the x-axis average positions $\mathbf{X}_u(t)$ and $\mathbf{X}_v(t)$ (bottom). From left to right: experiment $n = 11, 12, 14$ of Table 4.

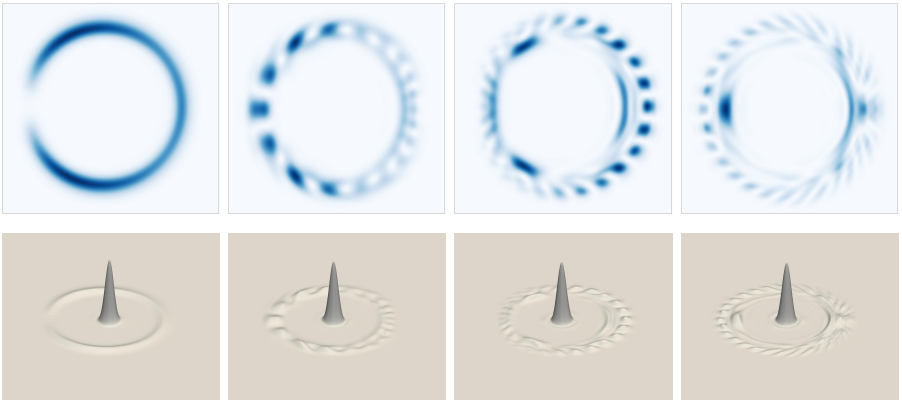

$t = 9.2 \cdot 10^{-3}$ $t = 2.48 \cdot 10^{-2}$ $t = 4.04 \cdot 10^{-2}$ $t = 5.6 \cdot 10^{-2}$

Figure 10: Density profile $|u(\mathbf{x},t)|^2$ (top row) and both profiles $|u(\mathbf{x},t)|^2$ and $|v(\mathbf{x},t)|^2$ (bottom) after consecutive re-collisions (experiment $n = 13$ of Table 4). Instants of velocity inversion.

species repulsion has a much stronger magnitude than the intra-species repulsion ($n = 16$).

In the former case in each cycle the phenomenon is qualitatively replicated, with more and more mass concentration arising in the course of the subsequent collisions, until when a proper blow-up occurs in the density profile of each component (its L^∞-norm diverges in finite time). In the latter case too the phenomenon is repeated almost periodically, thanks to the re-focusing effect of the trap, and at each new collision a new 'splash' takes place of one component against the other: the L^∞-norm of each components reaches its local maximum at the instants of largest spatial overlap at the centre of the trap, and its local minimum at the instants of velocity inversion, with such minima decreasing slightly at each cycle due to the mild focusing effect of the intra-component attraction.

Acknowledgements. This work was partially supported by the 2014-2017 MIUR-FIR grant "*Cond-Math: Condensed Matter and Mathematical Physics*", code RBFR13WAET.

References

[1] Anapolitanos, I., Hott, H., Hundertmark, D.: Derivation of the Hartree equation for compound Bose gases in the mean field limit. Rev. Math. Phys. **29**(7), 1750022, 28 (2017)
[2] Bao, W., Cai, Y.: Mathematical theory and numerical methods for Bose-Einstein condensation. Kinetic and Related Models **6**(1), 1–135 (2013)
[3] Bao, W., Jaksch, D.: An Explicit Unconditionally Stable Numerical Method for Solving Damped Nonlinear Schrödinger Equations with a Focusing Nonlinearity. SIAM Journal on Numerical Analysis **41**(4), 1406–1426 (2003)
[4] Bao, W., Jaksch, D., Markowich, P.A.: Numerical solution of the Gross–Pitaevskii equation for Bose–Einstein condensation. Journal of Computational Physics **187**(1), 318–342 (2003)
[5] Bao, W., Shen, J.: A Fourth-Order Time-Splitting Laguerre–Hermite Pseudospectral Method for Bose–Einstein Condensates. SIAM Journal on Scientific Computing **26**(6), 2010–2028 (2005)
[6] Berland, H., Owren, B., Skaflestad, B.: Solving the nonlinear Schrödinger equation using exponential integrators. Modeling, Identification and Control **27**(4), 201–217 (2006)
[7] Canuto, C., Hussaini, M. Y., Quarteroni, A., Zhang,T.: Spectral Methods, volume 1. Springer (2006)
[8] Chen, J., Guo, B.: Blow-up profile to the solutions of two-coupled Schrödinger equations. Journal of Mathematical Physics **50**(2) (2009)
[9] Chui, S. T., Ryzhov, V. N., Tareyeva, E. E.: Phase separation and vortex states in binary mixture of Bose-Einstein condensates in trapping potentials with displaced centers. Journal of Experimental and Theoretical Physics Letters **75**(5), 233–237 (2002)
[10] Fanelli, L., Montefusco, E.: On the blow-up threshold for weakly coupled nonlinear Schrödinger equations. J. Phys. A **40**(47), 14139–14150 (2007)
[11] Hall, D.S.: Multi-Component Condensates: Experiment, pages 307–327. Springer Berlin Heidelberg, Berlin, Heidelberg (2008)
[12] Hall, D.S., Matthews, M. E., Enscher, J.R., Wieman, C.E., Cornell, E.A.: The Dynamics of Component Separation in a Binary Mixture of Bose-Einstein Condensates. Phys. Rev. Lett. **81**(8), 1539–1542 (1998)

[13] Jüngel, A., Weishäupl, R.M.: Blow-up in two-component nonlinear Schrödinger systems with an external driven field. Mathematical Models and Methods in Applied Sciences **23**(09), 1699–1727 (2013)
[14] Lee, K.L., Jørgensen, N.B., Liu, I.K., Wacker, L., Arlt, J.J., Proukakis, N.P.: Phase separation and dynamics of two-component bose-einstein condensates. Phys. Rev. A **94** (2016)
[15] Li, X., Wu, Y., Lai, S.: A sharp threshold of blow-up for coupled nonlinear Schrödinger equations. Journal of Physics A: Mathematical and Theoretical **43**(16), 165205 (2010)
[16] Lin, T.C., Wei, J.: Solitary and self-similar solutions of two-component system of nonlinear Schrödinger equations. Physica D: Nonlinear Phenomena **220**(2), 99–115 (2006)
[17] Ma, L., Zhao, L.: Sharp thresholds of blow-up and global existence for the coupled nonlinear Schrödinger system. Journal of Mathematical Physics **49**(6) (2008)
[18] Malomed, B.: Multi-Component Bose-Einstein Condensates: Theory, pages 287–305. Springer Berlin Heidelberg, Berlin, Heidelberg (2008)
[19] Mancini, M.W., Telles, G.D., Caires, A.R.L., Bagnato, V.S., Marcassa, L.G.: Observation of Ultracold Ground-State Heteronuclear Molecules. Phys. Rev. Lett. **92** 133203, Apr (2004)
[20] Michelangeli, A., Nam, P.T., Olgiati, A.: Ground state energy of mixture of Bose gases, Rev. Math. Phys. **31** 1950005:58 (2019). doi:10.1142/S0129055X19500053
[21] Michelangeli, A., Olgiati, A.: Mean-field quantum dynamics for a mixture of Bose–Einstein condensates. Analysis and Mathematical Physics **7**(4), 377–416 Dec (2017)
[22] Modugno, G., Ferrari, G., Roati, G., Brecha, R.J., Simoni, A., Inguscio, M.: Bose-Einstein Condensation of Potassium Atoms by Sympathetic Cooling. Science **294**(5545), 1320–1322 (2001)
[23] Modugno, G., Modugno, M., Riboli, F., Roati, G., Inguscio, M.: Two Atomic Species Superfluid. Phys. Rev. Lett. **89**, 190404 (2002)
[24] Mueller, E.J., Ho, T.L., Ueda, M., Baym, G.: Fragmentation of Bose-Einstein condensates. Phys. Rev. A **74**, 033612 (2006)
[25] Olgiati, A.: Effective Non-linear Dynamics of Binary Condensates and Open Problems. In Gianfausto Dell'Antonio and Alessandro Michelangeli, editors, Advances in Quantum Mechanics: Contemporary Trends and Open Problems, Springer INdAM Series, pages 239–256. Springer International Publishing, (2017)
[26] Papp, S.B., Wieman, C.E.: Observation of Heteronuclear Feshbach Molecules from a ^{85}Rb-^{87}Rb Gas. Phys. Rev. Lett. **97**, 180404 (2006)
[27] Pitaevskii, L., Stringari, S.: Bose-Einstein Condensation and Superfluidity. Oxford University Press (2016)
[28] Salman, H.: A time-splitting pseudospectral method for the solution of the Gross–Pitaevskii equations using spherical harmonics with generalised-Laguerre basis functions. Journal of Computational Physics **258**, 185–207 (2014)
[29] White, A., Hennessy, T., Busch, T.: Emergence of classical rotation in superfluid Bose-Einstein condensates. Phys. Rev. A **93**, 033601 (2016)
[30] Xu, Q., Chang, Q.: New numerical methods for the coupled nonlinear Schrödinger equations. Acta Mathematicae Applicatae Sinica, English Series, **26**(2), 205–218 (2010)
[31] Zhang, Y., Bao, W., Li, H.: Dynamics of rotating two-component Bose–Einstein condensates and its efficient computation. Physica D: Nonlinear Phenomena **234**(1), 49–69 (2007)

Received: 26 May 2018.
Accepted: 23 November 2018.

Alessandro Michelangeli
SISSA, via Bonomea 265, 34136 Trieste, Italy.
alemiche@sissa.it

Giuseppe Pitton
SISSA, via Bonomea 265, 34136 Trieste, Italy.
gpitton@sissa.it